Backbone Dynamics of Tet Repressor α8∩α9 Loop †

ARTICLE *in* BIOCHEMISTRY · MARCH 2000

Impact Factor: 3.02 · DOI: 10.1021/bi9912591

Backbone Dynamics of Tet Repressor α8∩α9 Loop†

Benedetta Vergani,‡,§ Martin Kintrup,|| Wolfgang Hillen,|| Hans Lami,‡ Etienne Piémont,‡ Elisa Bombarda,‡,§ Patrizia Alberti,‡,§ Silvia M. Doglia,§ and Marie Chabbert*,‡,⊥

Laboratoire de Pharmacologie et Physicochimie, Centre National de la Recherche Scientifique UMR 7034, Faculté de Pharmacie, Université Louis Pasteur de Strasbourg, 74 route du Rhin, 67401 Illkirch, France, Dipartimento di Fisica, Università degli Studi di Milano, Via Celoria 16, 20133 Milano, Italy, and Lehrstuhl für Mikrobiologie, Institut für Mikrobiologie, Biochemie und Genetik, Friedrich-Alexander Universität Erlangen-Nürnberg, Staudtstrasse 5, 91058 Erlangen, Germany

Received June 2, 1999; Revised Manuscript Received October 15, 1999

ABSTRACT: A set of single Trp mutants of class B Tet repressor (TetR), in which Trp residues are located from positions 159 to 167, has been engineered to investigate the dynamics of the loop joining the α-helices 8 and 9. The fluorescence anisotropy decay of most mutants can be described by the sum of three exponential components. The longest rotational correlation time, 30 ns at 10 °C, corresponds to the overall rotation of the protein. The shortest two components, on the subnanosecond and nanosecond time scale, are related to internal motions of the protein. The initial anisotropy, in the 0.16−0.22 range, indicates the existence of an additional ultrafast motion on the picosecond time scale. Examination of physical models for underlying motions indicates that librational motions of the Trp side chain within the rotameric $\chi_1 \times \chi_2$ potential wells contribute to the picosecond depolarization process, whereas the subnanosecond and nanosecond depolarization processes are related to backbone dynamics. In the absence of inducer, the order parameters of these motions, about 0.90 and 0.80 for most positions, indicate limited flexibility of the loop backbone. Anhydrotetracycline binding to TetR induces an *increased* mobility of the loop on the nanosecond time scale. This suggests that entropic factors might play a role in the mechanism of allosteric transition.

Characterization of the dynamics of a protein is critical for a detailed understanding of its function and mechanism of action. Different spectroscopic methods, including NMR, fluorescence, and electron spin resonance, provide evidence for a variety of internal motions on time scales ranging from picosecond to seconds and longer (for a review, see ref *1*). Over the past 10 years, the development of multidimensional nuclear magnetic resonance allowed the description of the backbone dynamics of a variety of small ^{15}N-labeled proteins. It was soon found that the initial model proposed by Lipari and Szabo (*2*) to describe internal motion in proteins in terms of an effective rotational correlation time and a related order parameter did not take into account the complexity of protein dynamics (*3*, *4*). Recently, isotopic labeling strategies have been developed to obtain information about side chain dynamics (*5*, *6*). Multidimensional NMR is, however, limited to small proteins. Alternative approaches have to be developed for larger proteins.

Class B Tet repressor (TetR^B) regulates the transcription of the *Tn10*-encoded *tet* resistance determinant conferring resistance to tetracycline in gram-negative bacteria (for a review, see ref *7*). In the absence of tetracycline, TetR[1] prevents the expression of the resistance protein TetA and of TetR itself by binding to the *tetO$_1$* and *tetO$_2$* operators, which regulate the transcription of the *tetA* and *tetR* genes. Upon tetracycline binding, TetR undergoes a conformational change and dissociates from the operators, thereby allowing the synthesis of TetA, which exports tetracycline out of the bacteria. TetR^B is a homodimer of two 207-residue-long polypeptide chains. The crystallographic structure of the homologous TetR^D has been resolved, both in the presence and in the absence of inducer (*8*−*11*). Each monomer is composed of 10 α-helices. The α-helices 1−3 form the operator binding domain, which is connected to the core domain (α-helices 5 to 10) by α-helix 4. A seesaw motion of this helix may transduce information from the tetracycline binding domain to the operator binding domain. The tetracycline binding pocket in the core domain is formed by residues from both monomers. In the absence of tetracycline, the binding pocket is open due to a lateral motion of α-helix 9. Upon inducer binding, a "sliding door" motion of α-helix 9 closes the pocket to trap tetracycline inside the protein. Either in the absence (*10*) or in the presence of tetracycline or of its analogues (*8*, *9*), the only part of TetR^D whose structure cannot be resolved due to poorly defined electron density is the α8∩α9 loop connecting the α-helices 8 and 9. In the induced form (*9*), the loop extends from residues

† This work was supported in part by the Deutsche Forschungsgemeinschaft through SFD 473 to W.H. B.V., E.B., and P.A. were supported by the Erasmus scholarship program of the ECC.

* To whom correspondence should be addressed.
‡ Université Louis Pasteur de Strasbourg.
§ Università degli Studi di Milano.
|| Friedrich-Alexander Universität Erlangen-Nürnberg.
⊥ Present address: INSERM E 9928, CHU, 4 rue Larrey, 49033 Angers, France.

[1] Abbreviations: TetR, Tet repressor; AnTc, 5a,6-anhydrotetracycline; α8∩α9, loop joining the α-helices 8 and 9; HEPPS, 4-(2-hydroxyethyl)piperazine-1-propanesulfonic acid; Tris-HCl, tris(hydroxymethyl)aminomethane hydrochloride; β-ME, β-mercaptoethanol; fwhm, full width at half-maximum.

10.1021/bi9912591 CCC: $19.00
Published on Web 02/22/2000

$TetR^B$	Ala-Lys-Glu-Glu-Arg-Glu-Thr-Pro-Thr-Thr-Asp-Ser-Met-Pro	
$TetR^D$	Ala-Leu-Thr-Asp-Arg-Pro-Ala-Ala-Pro-Asp-Glu-Asn-Leu-Pro	
	154	167

FIGURE 1: Sequence of the α8∩α9 loop in induced TetR from classes B and D. The underlined residues were mutated to Trp.

154 to 167 and the electron density of the fragment 156−164 is not well defined. In the inducer-free form (*10*), α-helix 8 is one turn shorter and the poorly defined fragment includes residues 152−165. The mobility of this region is crucial for the mechanism of induction of TetR. Deletion mutants within this fragment have an induction-deficient $TetR^S$ phenotype, whereas Ala mutations do not affect inducibility (*12*, *13*). Engineered $TetR^D$ mutants with disulfide bonds between the α8∩α9 loop and the protein core (DC106PC159′ and EC107NC165′ $TetR^D$) are not inducible (*14*). To better understand the role of this loop in the mechanism of action of Tet repressor, it is necessary to investigate the dynamics of this important part of the protein.

The fluorescence of Trp residues is widely used to obtain information about the structure and dynamics of proteins. Although the information is limited to the site of the probe, the capability to introduce single Trp residues in strategic positions of a protein by molecular engineering makes fluorescence anisotropy a very interesting approach to study the dynamics of large proteins. A set of single Trp mutants of $TetR^B$, in which a Trp residue was positioned at each position from 159 to 167 in the α8∩α9 loop has been engineered (Figure 1). The set was not extended to the N-terminal part of the loop because mutations at positions 157 and 158 yield an impaired inducibility (*15*). The single Trp mutations at positions from 159 to 167 do not interfere with induction (*16*). In this report, we present a fluorescence anisotropy decay study of this set of single Trp mutants in the presence and in the absence of anhydrotetracycline. This study provides information on the backbone dynamics of the α8∩α9 loop and shows that it is affected by inducer binding.

MATERIALS AND METHODS

Materials. All the chemicals were of reagent grade or better. Ultrapure water (MilliQ instrument from Millipore Corp.) was used throughout the experiments. 5a,6-Anhydrotetracycline was from Jansen. The engineered single Trp mutants of class B Tet repressor used in this study, Y43F75Wxxx TetR, where xxx was the position of the Trp residue and ranged from 159 to 167, were purified as described elsewhere (*17*). The Y43F75 TetR mutant was prepared according to the same protocol. Its fluorescence was free of detectable Trp contamination, indicating a high spectroscopic purity. The proteins were stored at −18 °C in 50% (v/v) glycerol. The time-resolved measurements were carried out in a buffer containing 10 mM HEPPS, pH 8.0, 100 mM NaCl, 5 mM $MgCl_2$, and 10 mM β-mercaptoethanol (β-ME). Steady-state measurements were carried out in buffers containing either 10 mM HEPPS, pH 8.0, or 10 mM Tris-HCl, pH 8.0, 100 mM NaCl, 5 mM $MgCl_2$, and 10 mM β-ME. There was no significant difference between the two buffers.

The affinity of the Trp mutants for AnTc was similar to that of Y43F75 TetR (K_D of about 10^{11} M^{-1}), indicating that the Trp mutations did not interfere with the inducer binding (*16*). The preparations were, however, contaminated by a small amount of inactive protein with impaired inducer binding. Due to an efficient energy transfer from Trp to AnTc, the fluorescence intensity of any Trp mutant was strongly quenched upon addition of AnTc (see Results). The presence of inactive protein was evident for mutants with very high energy transfer efficiency ($F/F_0 \leq 0.10$). For these mutants, 70% or more of the fluorescence was statically quenched in the presence of a saturating amount of AnTc. When the decay of the residual fluorescence was analyzed, the lifetime spectrum obtained with the maximum entropy method (MEMSYS2 software, MEDC Ltd.) (*18*) was the superposition of a subnanosecond lifetime distribution corresponding to energy-transferring Trp and of a trimodal lifetime distribution similar to that obtained in the absence of AnTc (*19*). This indicates the presence of a small amount (<10%) of inactive protein unable to bind AnTc. Due to the relative quantum yields of the AnTc-bound and AnTc-free TetR mutants, most of the fluorescence should arise from this inactive protein when the energy transfer is very efficient. The contamination of wild-type TetR preparations by similar amounts of inactive protein (5−10%) has also been observed (W. Hillen, personal communication), indicating that this is not due to a specific effect of the mutations introduced in the proteins.

Spectroscopic Methods. The concentrations were determined spectrophotometrically. The molar extinction coefficient of AnTc was 11 600 M^{-1} cm^{-1} at 430 nm. UV absorption spectra were recorded on a Cary 4 spectrophotometer. Steady-state fluorescence measurements were carried out either with a MPF66 spectrofluorometer (Perkin-Elmer) or with a Fluorolog 1680 spectrofluorometer (Spex). Spectra were corrected for the buffer baseline, the instrumental excitation and emission wavelength dependence, and for the screening effect due to the absorption of AnTc when present. Excitation polarization spectra were monitored with an SLM 8000 spectrofluorometer (T-format device) at an emission wavelength set at 355 nm with interferential filters.

Time-resolved anisotropy measurements were carried out with the pulse fluorometry technique, with a Ti−Sa laser as excitation source (*19*). The excitation and emission wavelengths were 295 and 350 nm, respectively. The calibration of the Ortec 921 multichannel analyzer was 25.5 ps/channel. The emission beam was vertically polarized. The polarization of the excitation beam was changed by using a quartz crystal rotating the beam polarization of 90° at the excitation wavelength. The fluorescence decays with vertical and horizontal excitation polarization, $I_{ver}(t)$ and $I_{hor}(t)$, were alternatively recorded (typically, 10 × 2 times). The excitation polarization was changed when the total number of counts (TNC) reached a prefixed value (typically, 500 000 for vertical excitation and 400 000 for horizontal excitation). This procedure avoided biases due to (1) shifts in the response function position when the vertical and horizontal decays were separately recorded and (2) changes in the beam intensity when alternative measurements were carried out without precounting. Moreover, a homemade automatic device shut off the excitation beam when its intensity was ≤90% of the maximum intensity to ensure very stable excitation pulses. The full width at half-maximum (fwhm) of the excitation pulse was about 40 ps.

Table 1: Analysis of Typical Anisotropy Decays[a]

	n	r_1	θ_1	r_2	θ_2	r_3	θ_3	Σ^2	*P*
W162	2	0.047 ± 0.003	1.96 ± 0.24	0.144 ± 0.003	22.5 ± 1.1			0.0291	0.00015
	3	0.022 ± 0.005	0.27 ± 0.11	0.059 ± 0.015	3.95 ± 1.26	0.121 ± 0.017	30.2 ± 7.6	0.0282	
W161	2	0.036 ± 0.003	1.64 ± 0.30	0.133 ± 0.003	35.5 ± 2.6			0.0532	0.15
	3	0.014 ± 0.007	0.16 ± 0.16	0.034 ± 0.004	2.13 ± 0.69	0.131 ± 0.005	37.6 ± 4.5	0.0619	

[a] Parameters (±SE) obtained for the best fits of the Trp-161 and Trp-162 anisotropy decays. The decays were analyzed according to eq 2. Σ^2 represents the absolute sum of squares and *n* the number of exponential components. The *P* value was determined by the *F*-test. The measurements were carried out at 10 °C, in 10 mM HEPPS, pH 8.0, 100 mM NaCl, 5 mM $MgCl_2$, and 10 mM β-ME. The concentrations of Y43F75W161 and Y43F75W162 TetR were 9 μM (monomers).

The deconvolution method (*20*) widely used to analyze the anisotropy decay data could not be implemented here. This approach, which involves the deconvolution of the experimental I_{ver} and I_{hor} decays, requires similar time scales for the fluorescence intensity and anisotropy decays. This requirement was not filled here. The average lifetime of the fluorescence decay was between 2.5 and 3.8 ns at 10 °C for any of the Trp, whereas the anisotropy decay had a large contribution from a 30 ns component (see Results). As a result of this order of magnitude difference in the time scales, the long component could not be adequately recovered by the reconvolution procedure and the anisotropy decay parameters obtained by this method made no scientific sense.

To overcome this difficulty, we directly analyzed the anisotropy decays obtained from the experimental $I_{ver}(t)$ and $I_{hor}(t)$ decays:

$$r(t) = [I_{ver}(t) - G\, I_{hor}(t)]/[I_{ver}(t) + 2G\, I_{hor}(t)] \quad (1)$$

with *G* equal to $TNC_{ver}(1 - r_{st})/TNC_{hor}(1 + 2r_{st})$. The static anisotropy r_{st} was measured with the same device at very low counting rate (<1 kHz) (*21*). The anisotropy decays were analyzed as sums of exponential components, defined by their rotational correlation times θ_i and their preexponential terms r_i:

$$r(t) = \sum_i r_i\, e^{-t/\theta i} \quad (2)$$

by using a nonlinear least-squares procedure. Goodness of fit was quantified by the sum-of-squares. *F*-tests (*22*) were performed to compare goodness of fits and determine whether the decrease in the sum-of-squares with additional variables was significant. The *P* value calculated by the *F*-test indicates the probability that the decrease in the sum-of-squares is due to chance. A low *P* value indicates that the more complicated model is significantly better than the simpler model.

The validity of this approach was verified by analyzing the anisotropy decay of TetR Trp-43. The deconvolution method has been applied successfully to this Trp whose anisotropy and fluorescence decays are on the same time scale (about 3 ns) (*23*). The parameters obtained by direct analysis of $r(t)$ ($r_1 = 0.047 \pm 0.008$, $r_2 = 0.135 \pm 0.002$, $r_\infty = 0.029 \pm 0.001$, $\theta_1 = 0.10 \pm 0.03$ ns, $\theta_2 = 3.5 \pm 0.1$ ns) were fully consistent with those obtained by the deconvolution analysis of $I_{ver}(t)$ and $I_{hor}(t)$ ($r_1 = 0.041 \pm 0.010$, $r_2 = 0.131 \pm 0.004$, $r_\infty = 0.028 \pm 0.004$, $\theta_1 = 0.18 \pm 0.08$, $\theta_2 = 3.6 \pm 0.3$) (*23*). This indicates that, at the precision that can be reached by either analysis approach, they yield similar results, thanks to the narrowness of the response function.

The Y43F75W170 TetR mutant was used to measure the rotational correlation time of the protein. The single Trp residue of this mutant, at position 170, was located within the hydrophobic core of the protein. Its anisotropy decay was biexponential with a long rotational correlation time representing about 95% of the total amplitude. The overall rotational correlation time of TetR, 30 ± 2 ns at 10°, was determined from the best fit of this long rotational correlation time as a function of the temperature. The limit anisotropy of *N*-acetyl-L-tryptophanamide (NATA) was measured under the same excitation conditions ($\lambda_{ex} = 295$ nm) at −170 °C in an organic glass (EPA) obtained by mixing diethyl ether, isopentane, and ethanol (5/5/2 v/v/v).

RESULTS

(1) Anisotropy Decay Analysis. The anisotropy decays of Trp-162 and Trp-161 are shown in Figures 2a and 3a. These decays were analyzed according to eq 2 with an increasing number of exponentials until the fit no longer improved (Table 1). The best biexponential fit of Trp-162 with rotational correlation times of 2.0 ± 0.2 and 22 ± 1 ns was not satisfying, with a significant deviation of the residuals at short times (Figure 2b). The three-component analysis yielded a random distribution of the residuals (Figure 2c). The rotational correlation times, 0.3 ± 0.1, 3.9 ± 1.3, and 30 ± 8 ns, were separated by an order of magnitude. The low *P* value (0.00015) obtained with the *F*-test indicates that the three-component model is significantly better than the two-component model. Moreover, the long rotational correlation time obtained with the triexponential analysis matched the overall rotational correlation time of TetR, 30 ± 2 ns, which was independently determined with the Y43F75W170 mutant (see Materials and Methods). The long rotational correlation time obtained with two component analysis, 22 ± 1 ns, was markedly shorter than the repressor overall rotational correlation time, which could not be easily explained.

On the other hand, the anisotropy decay of Trp-161 could be described as the sum of two exponential components with rotational correlation times of 1.6 ± 0.3 and 35 ± 3 ns. The deviation of the residuals at short times was too small to be significant (Figure 3b). The distribution of the residuals did not significantly improve upon the addition of a third component (Figure 3c). The longest two components were not significantly altered, whereas the amplitude of the additional subnanosecond component represented less than 10% of the total amplitude. The *P* value obtained with the *F*-test, 0.15, indicates that the three-component analysis is not significantly better than the two-component analysis.

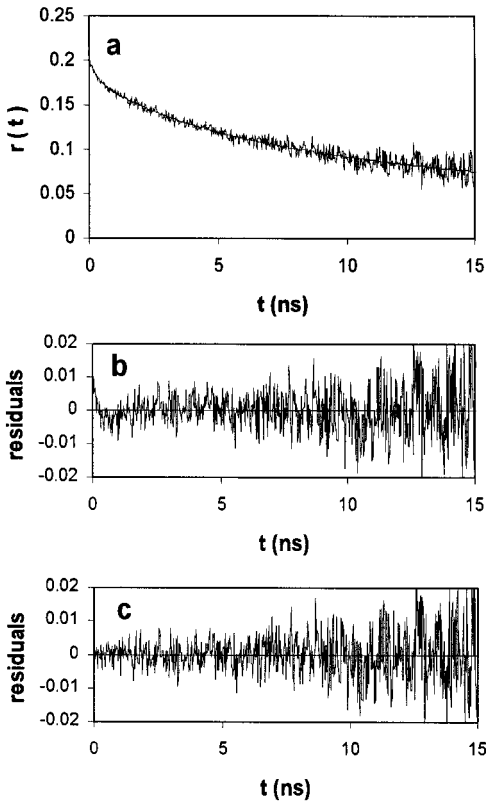

FIGURE 2: Fluorescence anisotropy decay of Trp-162 in inducer-free Y43F75W162 TetR. (a) The solid line corresponds to the best triexponential fit. Also shown are plots of the residuals (b) for the best biexponential fit and (c) the best triexponential fit. The measurement was carried out in 10 mM HEPPS−HCl pH 8.0, 100 mM NaCl, 5 mM $MgCl_2$, and 10 mM β-ME at 10°C with a protein concentration of 9 μM (monomers).

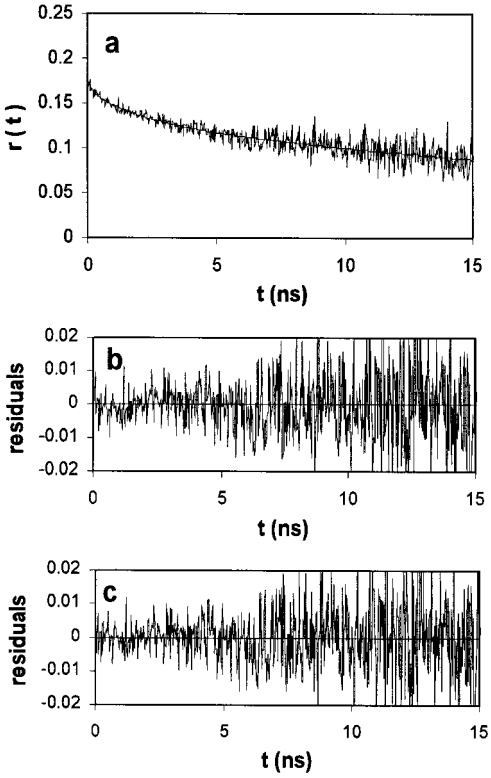

FIGURE 3: Fluorescence anisotropy decay of Trp-161 in inducer-free Y43F75W161 TetR. (a) The solid line corresponds to the best biexponential fit. Also shown are plots of the residuals for (b) the best biexponential fit and (c) the best triexponential fit. The measurement was carried out in 10 mM HEPPS−HCl, pH 8.0, 100 mM NaCl, 5 mM $MgCl_2$, and 10 mM β-ME at 10°C with a protein concentration of 9 μM (monomers).

The analyzed anisotropy decay is a function of the observed vertical and horizontal fluorescence decays, which are convolution products of the intrinsic vertical and horizontal decays with the device response function (fwhm 40 ps). This might lead to a distortion of the anisotropy decay curve as compared to the true anisotropy decay, which might alter the beginning of the decay curve. However, since the response function is narrow, this should not alter the decay observed for $t \gg 40$ ps. The anisotropy decay of Trp-162 provides an example of both a better fit at short times (Figure 2c) and a physical interpretation of the long rotational correlation time upon the addition of a third component. The absence of a significant subnanosecond component for Trp-161 indicates that, when it is present, the additional short component does not result from distortion of the observed anisotropy decay but must have a physical meaning. Control analysis of biexponential decays with a subnanosecond component (e.g., TetR Trp-43; see Materials and Methods) corroborates the assumption that the response function is narrow enough to avoid significant distortion of the recovered decay parameters, at the precision of the analysis.

(2) Anisotropy Decays in the Inducer-Free State. The multiexponential analysis of Trp-161 and Trp-162 indicates the existence of one or two internal motions independent of the overall motion. By analogy with NMR motional parameters (*4*), each motion can be described by its rotational correlation time and its order parameter. Equation 2 was rewritten as

$$r(t) = r_0 e^{-t/\theta_c}(S_s^2 S_f^2 + S_f^2(1 - S_s^2)e^{-t/\theta_s} + (1 - S_f^2)\, e^{-t/\theta_f}) \quad (3)$$

with $\theta_c = \theta_1$, $1/\theta_s = 1/\theta_2 - 1/\theta_c$, $1/\theta_f = 1/\theta_3 - 1/\theta_c$, $r_0 = r_1 + r_2 + r_3$, $S_f^2 = (r_2 + r_3)/r_0$, and $S_s^2 = r_3/(r_2 + r_3)$. S_s^2 and S_f^2 are the order parameters that characterize the slow and fast internal motions. The two-component analysis was equivalent to S_f^2 (or S_s^2) = 1. All the decays were analyzed as sums of two and three components with a long rotational correlation time fixed to a constant value of 30 ns. This value corresponds to the overall rotational correlation time of the protein dimer and must be present in the anisotropy decay. This did not alter the goodness of fit, with virtually identical residuals, but reduced the uncertainties on the other decay parameters (not shown). The adequate model was determined with the *F*-test. The third component analysis was selected when the *P* value was <0.05.

The anisotropy decay parameters are reported in Table 2. Three components were required to adequately describe the fluorescence anisotropy decays of most Trp. There were two exceptions, Trp-161 and Trp-167, whose fit did not significantly improve upon the addition of a third component. However, this corresponded to two different situations. Trp-161 was characterized by the absence of a significant subnanosecond component. The anisotropy decay of Trp-167 could be adequately described by two components on the 0.4 and 30 ns time scales. This indicates the absence of motion with significant amplitude on the nanosecond time scale ($S_s^2 = 1$) and might be related to the peculiar

Table 2: Analysis of the Trp Anisotropy Decays in the Absence of AnTc[a]

Trp	*n*	r_0	θ_f (ns)	S_f^2	θ_s (ns)	S_s^2	*P*
159	3	0.208 ± 0.006	0.21 ± 0.17	0.90 ± 0.04	1.7 ± 0.4	0.80 ± 0.03	0.04
160	3	0.212 ± 0.004	0.38 ± 0.17	0.88 ± 0.03	3.5 ± 0.8	0.83 ± 0.02	0.0002
161	2	0.172 ± 0.003			1.1 ± 0.2	0.81 ± 0.01	0.44
162	3	0.203 ± 0.006	0.23 ± 0.12	0.90 ± 0.03	4.1 ± 0.4	0.68 ± 0.01	0.0007
163	3	0.218 ± 0.006	0.26 ± 0.17	0.91 ± 0.03	3.7 ± 0.7	0.79 ± 0.02	0.017
164	3	0.164 ± 0.005	0.21 ± 0.14	0.88 ± 0.04	1.7 ± 0.3	0.72 ± 0.03	0.014
165	3	0.169 ± 0.007	0.25 ± 0.18	0.89 ± 0.04	3.9 ± 1.0	0.78 ± 0.02	0.022
166	3	0.212 ± 0.006	0.30 ± 0.18	0.88 ± 0.04	2.4 ± 0.8	0.84 ± 0.03	0.023
167	2	0.199 ± 0.003	0.44 ± 0.12	0.90 ± 0.02			0.67

[a] Parameters (±SE) obtained for the best fits of the anisotropy decays. The decays were analyzed according to eq 3. The overall rotational correlation time, θ_c, was fixed to the constant value of 30 ns. The adequate number of exponential components, *n*, was determined by the *P* value obtained with the *F*-test, upon comparison of the goodness of the biexponential and triexponential fits. The threshold was set at 0.05. The measurements were carried out at 10 °C, in 10 mM HEPPS pH 8.0, 100 mM NaCl, 5 mM $MgCl_2$, and 10 mM β-ME. The protein concentrations ranged from 7 to 12 μM.

environment of this residue, which is located at the C-terminal end of the α8∩α9 loop, near Pro-168 (first residue of α-helix 9).

For Trp residues located elsewhere, the triexponential fit of the anisotropy decay was significantly better than the biexponential fit. This indicates the existence of two internal motions with different time scales. The fast internal rotational correlation, θ_f, was on the subnanosecond time scale (0.3 ± 0.1 ns) and could not be measured precisely. The order parameter associated with this motion, S_f^2, was in the 0.88−0.91 range for all the Trp investigated. The slow internal rotational correlation time, θ_s, was on the nanosecond time scale (3 ± 1 ns). For most Trp positions, the order parameter of this nanosecond motion was in the 0.78−0.84 range. Two positions, 162 and 164, had markedly lower nanosecond order parameters (0.68 and 0.72, respectively). The low S_s^2 of Trp-164 was associated with one of the shortest rotational correlation times (1.7 ns). This position corresponded to the fastest anisotropy-decaying Trp.

Whichever the Trp investigated, the initial anisotropy was markedly lower than the limit anisotropy of NATA in an EPA glass at −170 °C, which is equal to 0.27. This indicates the presence of an additional ultrafast motion on the subpicosecond/picosecond time scale that cannot be observed with our device (θ_{uf} < 50 ps). For most residues, the initial anisotropy was in the 0.20−0.22 range. Three Trp residues, 161, 164, and 165, had an initial anisotropy markedly lower ($0.164 < r_0 < 0.172$). This might be due either to a larger amplitude of the ultrafast motion or to a shift in the excitation polarization spectra. The absence of significant shift in the excitation polarization spectra (e.g., Trp-165 and Trp-163, Figure 4) indicates that the decrease in the initial anisotropy is related to an increased amplitude of the ultrafast motion. The order parameter of this ultrafast motion is equal to $S_{uf}^2 = r_0/0.27$ (*24*), under the reasonable assumption that these Trp have the same limit anisotropy as NATA (*25*). The 0.20−0.22 range for the initial anisotropies correspond to an ultrafast order parameter in the 0.75−0.80 range.

The low ultrafast order parameter, S_{uf}^2, of Trp-161 (0.64) along with the absence of significant subnanosecond component at this position strongly suggests that the motion usually associated with the subnanosecond component was faster and contributed to the ultrafast picosecond depolarization. The subnanosecond components of Trp-164 and Trp-165 were similar to those observed for the other positions

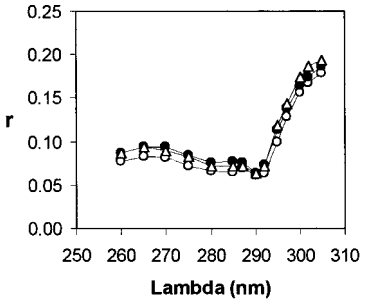

FIGURE 4: Excitation polarization spectra of Y43F75W163 TetR in the absence of AnTc (△) and of Y43F75W165 TetR in the absence of AnTc (○) and in the presence of a saturating amount of AnTc (●). Measurements were carried out in 10 mM Tris-HCl, pH 8.0, 100 mM NaCl, 5 mM $MgCl_2$, and 10 mM β-ME at 20 °C. The emission wavelength was 355 nm.

Table 3: Fluorescence Parameters of the Trp Mutants[a]

	λ_{max} (−AnTc)	λ_{max} (+AnTc)	F/F_0
159	346 ± 1	350 ± 1	0.38 ± 0.02
160	349 ± 1	352 ± 2	0.13 ± 0.02
161	347 ± 1	349 ± 2	0.09 ± 0.02
162	349 ± 1	352 ± 1	0.24 ± 0.02
163	344 ± 1	346 ± 2	0.10 ± 0.02
164	349 ± 1	349 ± 1	0.24 ± 0.02
165	347 ± 1	351 ± 1	0.43 ± 0.02
166	341 ± 1	341 ± 2	0.05 ± 0.02
167	344 ± 1	344 ± 1	0.25 ± 0.02

[a] The measurements were carried out at 20 °C, in 10 mM HEPPS, pH 8.0, 100 mM NaCl, 5 mM $MgCl_2$, and 10 mM β-ME. The excitation wavelength was 295 nm. The relative fluorescence intensity decrease upon addition of an excess of AnTc, F/F_0, was determined from the ratio of the area under the spectrum, after correction for the baseline and screening effects.

($S_f^2 \approx 0.89$) and their low ultrafast order parameters (0.61 and 0.63 for Trp-164 and Trp-165, respectively) should not be due to an additional contribution from other motions but to a larger amplitude of the picosecond motions.

The emission spectra of Trp-163, Trp-166, and Trp-167 (341 nm ≤ λ_{max} ≤ 344 nm) were blue-shifted as compared to the other positions (346 nm ≤ λ_{max} ≤ 349 nm) (Table 3). Two Trp with markedly different emission spectra, Trp-160 (λ_{max} = 349 nm) and Trp-166 (λ_{max} = 341 nm), had very similar anisotropy decays (Table 2). On the other hand, the three Trp with the most red-shifted emission spectra (Trp-160, Trp-162, and Trp-164) had different anisotropy decays. This indicates the absence of apparent correlation between the Trp depolarization process and the spectrum position,

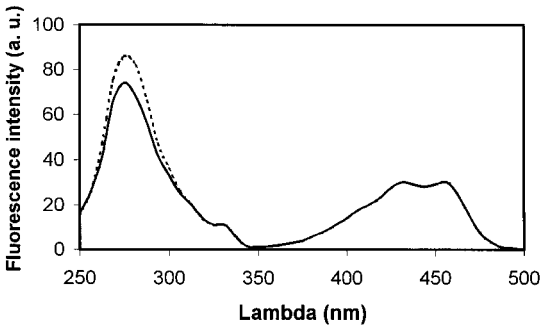

FIGURE 5: Fluorescence excitation spectra of AnTc bound to Y43F75 TetR (—) and to Y43F75W162 TetR (- - -). Measurements were carried out in 10 mM Tris-HCl, pH 8.0, 100 mM NaCl, 5 mM $MgCl_2$, and 10 mM β-ME at 20 °C. The emission wavelength was 520 nm. Spectra were normalized at 430 nm. The repressor concentrations were 1 μM (monomers). The molar ratio of AnTc to protein monomer was 0.5.

suggesting that solvent accessibility is not determinant for the dynamics of these Trp side chains (*26*).

(3) Anisotropy Decays in the Complex with Anhydrotetracycline. The dynamics of the α8∩α9 loop upon inducer binding was studied with AnTc rather than with tetracycline because of its lower overlapping integral with Trp (*23*). However, the fluorescence intensity of any of the Trp mutants dramatically decreased upon addition of AnTc. The amplitude of the relative fluorescence decrease (F/F_0) was dependent on the Trp position and ranged from 0.43 for Trp-165 to 0.95 for Trp-166 (Table 3). This dramatic effect was due to an efficient energy transfer from Trp to AnTc whose emission and absorption spectra partially overlap (*23*). The Trp to AnTc energy transfer is evident when the excitation spectra of AnTc bound to the Y43F75 TetR mutant and to a Trp-containing mutant are compared (e.g., Y43F75W162 TetR, Figure 5). The Förster distance for the Trp to AnTc energy transfer is about 22 Å (*23*). Preliminary modeling of the α8∩α9 loop indicates that the distances between the indole moieties and the center of the AnTc BCD chromophore should be in the 10−25 Å range, depending upon the position and the Trp rotamer considered (not shown). This is consistent with the energy transfer efficiencies, roughly estimated from the relative fluorescence decrease ($E = 1 - F/F_0$). AnTc binding also induced a red shift in the emission spectrum of some Trp (positions 159, 162, and 165) (Table 3). This might be related to an increased exposure of these Trp side chains to solvent, but a trivial effect due to different energy transfer efficiencies for different rotamers of a Trp side chain cannot be ruled out.

The anisotropy decays in the presence of AnTc were investigated at positions for which the energy transfer efficiency was less than 0.80 (159, 162, 164, 165, and 167) to avoid significant contribution from inactive unbound repressor (see Materials and Methods). The anisotropy decay of Trp-162 in the presence of AnTc is shown in Figure 6a. This decay was markedly faster that that obtained in the absence of AnTc (Figure 2a). Analysis of the anisotropy decay was carried out according to eq 3. The biexponential fit was very poor, with a marked deviation of the residuals up to 5 ns after the excitation pulse (Figure 6b), whereas the triexponential fit was satisfying (Figure 6c). Similar behavior was observed for Trp-159, -164, and -165 (not shown). This was corroborated by the very low P values

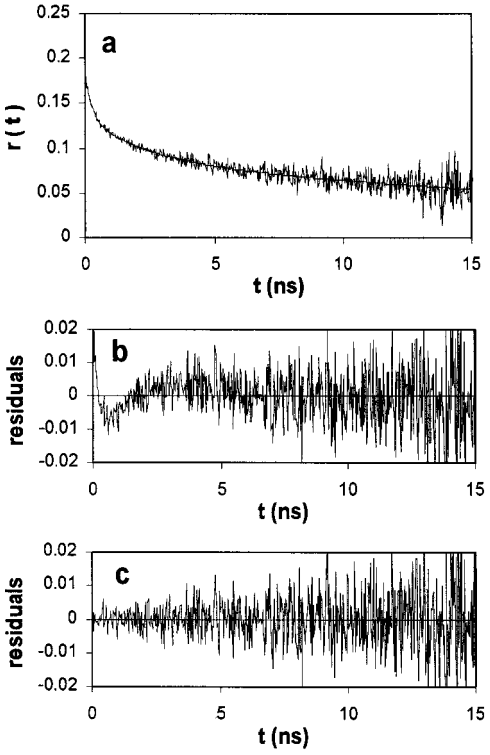

FIGURE 6: Fluorescence anisotropy decay of Trp-162 at 10 °C in AnTc-bound Y43F75W162 TetR. (a) The solid line corresponds to the best triexponential fit. Also shown are plots of the residuals for (b) the best biexponential fit and (c) the best triexponential fit. The concentration of Y43F75W162 TetR was 9 μM (monomers) and the molar ratio of AnTc to TetR monomers was 1.6. The measurement was carried out in 10 mM HEPPS−HCl, pH 8.0, 100 mM NaCl, 5 mM $MgCl_2$, and 10 mM β-ME at 10 °C.

(<0.001) (Table 4), which indicate that the improved fit upon the addition of a third component was very significant.

The increased difference in the goodness of the biexponential and triexponential fits as compared with the inducer-free protein can be related to the increased amplitude of the subnanosecond depolarization process (Table 4). For these four Trp, the subnanosecond order parameters, S_f^2, markedly decreased from about 0.90 in the absence of AnTc to 0.82 or less in its presence. The average of the associated subnanosecond rotational correlation times was 0.20 ± 0.04 ns. The uncertainties on the fast rotational correlation times were too large to observe significant changes as compared to the unbound state (0.3 ± 0.1 ns). AnTc binding also induced a marked decrease either in the nanosecond order parameter, S_s^2 (positions 159, 164, and 165) and/or in the nanosecond rotational correlation time, θ_s (positions 162 and 165) (Table 4). For these four Trp, θ_s was about 2.0 ± 0.5 ns and S_s^2 was ≤0.66. The order parameter associated with the ultrafast motion, S_{uf}^2, significantly increased upon AnTc binding at positions 164 and 165 from less than 0.63 to more than 0.72 (Tables 2 and 4). This is not due to a shift in the excitation polarization spectra (e.g., Trp-165; Figure 3) but indicates a decreased amplitude of the ultrafast motion. Trp-159 and Trp-162 did not have significant changes in S_{uf}^2 upon AnTc binding.

Trp-167 had a different behavior. As in the absence of AnTc, its decay could be described by a biexponential law. The amplitude of the internal motion was markedly larger than in the absence of AnTc, with an order parameter of

Table 4: Analysis of the Trp Anisotropy Decays in the Presence of AnTc[a]

Trp	*n*	r_0	θ_f (ns)	S_f^2	θ_s (ns)	S_s^2	*P*
159	3	0.216 ± 0.008	0.20 ± 0.08	0.77 ± 0.04	2.1 ± 0.5	0.61 ± 0.02	0.0001
162	3	0.187 ± 0.006	0.25 ± 0.06	0.72 ± 0.03	2.5 ± 0.3	0.66 ± 0.02	0.0001
164	3	0.202 ± 0.009	0.18 ± 0.09	0.79 ± 0.05	1.6 ± 0.3	0.57 ± 0.03	0.0008
165	3	0.195 ± 0.008	0.17 ± 0.08	0.82 ± 0.04	2.3 ± 0.4	0.63 ± 0.02	0.0008
167	2	0.203 ± 0.004			0.8 ± 0.1	0.72 ± 0.02	0.56

[a] Parameters (±SE) obtained for the best fits of the anisotropy decays. The decays were analyzed according to eq 3. The overall rotational correlation time, θ_c, was fixed to the constant value of 30 ns. The adequate number of exponential components, *n*, was determined by the *P* value obtained with the *F*-test, upon comparison of the goodness of the biexponential and triexponential fits. The threshold was set at 0.05. The measurements were carried out at 10 °C, in 10 mM HEPPS, pH 8.0, 100 mM NaCl, 5 mM $MgCl_2$, and 10 mM β-ME. The protein concentrations ranged from 7 to 12 μM. The molar ratio of AnTc to protein monomers was 1.6 ± 0.2.

0.72 (to be compared to 0.90), but the rotational correlation time was longer, on the nanosecond time scale (0.8 ± 0.1 ns). This led to an anisotropy decay faster than in the absence of AnTc but without the marked increase in the amplitude of the subnanosecond component observed for the other positions.

It is worth noting that energy transfer might induce an artifactual slowing down of anisotropy decays (*27*). In the present study, the changes observed correspond to faster anisotropy decays, which rule out the possibility of trivial energy transfer effects.

DISCUSSION

(1) Underlying Motions. The interpretation of anisotropy decays in terms of underlying motions relies on "the elementary observation that all motions effective in producing structural changes in proteins are rotations or oscillations about chemical bonds" (*1*). The orientation of the indole ring can be altered by changes in the χ_1 and χ_2 dihedral angles, due to rotations about the $C^\alpha-C^\beta$ and $C^\beta-C^\gamma$ bonds, or by changes in the orientation of the $C^\alpha-C^\beta-C^\gamma$ axis, due to changes in the Ramachandran angles φ and ψ of the local protein backbone. Preferential rotameric orientations of the Trp-162, Trp-163, and Trp-165 side chains with slow interconversion rates on the nanosecond time scale have been observed by time-resolved fluorescence (*19*). Similar triexponential decays were observed for any Trp in the 159−167 fragment (unpublished results). The absence of interconversion between the Trp rotamers on the fluorescence time scale is consistent with the high order parameters measured for each individual motion since such a mechanism would yield low order parameters (*28*). This is corroborated by NMR data, which indicate that interconversion between rotamers of Trp side chains in peptides and proteins is usually slow, on the microsecond to millisecond time scale (*29*−*31*).

The presence of noninterconverting Trp rotamers on the nanosecond time scale implies (i) that the rotations about the $C^\alpha-C^\beta$ and $C^\beta-C^\gamma$ bonds are limited to librational motions within the $\chi_1 \times \chi_2$ isomerization potential wells, which occur on the picosecond time scale or faster (*32*, *33*), and (ii) that the subnanosecond and nanosecond depolarization processes result from the changes in the orientation of the $C^\alpha-C^\beta-C^\gamma$ axis due to local motions of the protein backbone. The ultrafast depolarization process is thus related to librational motions of both the Trp side chain and the local protein backbone whereas the subnanosecond and nanosecond Trp depolarization processes are related to the local flexibility of the protein backbone. This interpretation of the anisotropy decay is similar to the assumption widely used in NMR that the extent of motion of the NH and $C^\alpha H$ vectors is a measure of the local backbone flexibility (*34*). It is consistent with the absence of correlation between Trp dynamics and spectra position (see Results).

Backbone motions monitored by NMR are usually described by an ultrafast component (<20 ps), observed for any residue in a protein, and by a nanosecond component, usually observed only for residues located within loops or at the N- and C-termini (*4*, *35*, *36*). This nanosecond component is usually related to transition between conformational substates (*4*). In addition to the ultrafast motion, the description of the α8∩α9 backbone motion requires both a nanosecond and a subnanosecond component. The hierarchical organization of the conformational substates of a protein, proposed by Frauenfelder et al. (*37*, *38*) from experimental studies on myoglobin, has been inferred by theorical and computational studies (*39*−*44*). The subnanosecond and nanosecond motions can be depicted as transitions between conformational substates of different hierarchical levels. The two-component backbone dynamics observed for the α8∩α9 loop is probably not specific to this loop. It could be observed by fluorescence because of an improved time resolution as compared to NMR and a protein overall rotational correlation time (30 ns) markedly larger than that of proteins studied by NMR (typically 5−10 ns), which makes easier the observation of two internal motions.

(2) Backbone Dynamics of the α8∩α9 Loop in the Inducer-Free State. The Lipari−Clore model used to interpret NMR data (*4*) corresponds to the limit of eq 3 when S_f^2 tends to 1, i.e., to a two-exponential analysis. Backbone motions of residues located within loops, as observed by NMR, are usually on the nanosecond time scale (typically from 0.5 to 4 ns) (*4*, *35*, *36*). The short components obtained from the biexponential analysis of the anisotropy decays ranged from 0.8 to 3 ns (e.g., Trp-161 and Trp-162, Table 1) and were consistent with NMR data for loop residues. The generalized order parameter for the subnanosecond/nanosecond motions measured by anisotropy, $S_g^2 = S_f^2 S_s^2$, can be qualitatively compared with the order parameters obtained by NMR. Order parameters for the nanosecond backbone motion of residues located within loops may be as low as 0.4 for "disordered" loops, e.g., IL-1β (*4*), or near 0.9 for "rigid" loops, e.g., IL-8 (*34*). In the absence of inducer, most of the residues within the 159−167 fragment had $0.70 < S_g^2 < 0.90$ (Figure 7). The only exceptions were residues 162 and 164 with S_g^2 values of 0.61 and 0.63, respectively. This indicates that the backbone of the α8∩α9 loop is not disordered but experiences moderate flexibility. This is still more evident when

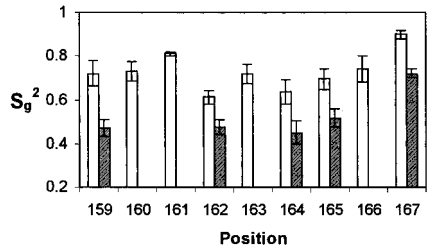

FIGURE 7: Generalized order parameter for the subnanosecond/nanosecond motions in the absence (open bars) and in the presence of AnTc (shaded bars).

individual motions are examined. The order parameter for the subnanosecond motions (about 0.90 in the absence of AnTc) corresponded to a reorientation angle of 20° between two equally populated states (*45*). For nanosecond motions, the reorientation angles ranged between 28° (Trp-166) and 40° (Trp-162). These values indicate that the subnanosecond and nanosecond motions correspond to conformational changes of limited amplitude.

The moderate flexibility of the $TetR^B$ α8∩α9 loop backbone is in apparent contrast with the poorly defined electron density of this loop in $TetR^D$ (*8*−*10*), which suggests a disordered structure. The $TetR^B$ backbone mobility on the nanosecond/subnanosecond time scale is rather uniform on the 159−166 range, except at position 164, which is significantly more mobile. Anisotropy decays at positions 160 and 166 were very similar, indicating similar backbone flexibilities. In $TetR^D$ crystals, the electron density was well-defined for position 166 but not for position 160. The sequences of the α8∩α9 loops from the two TetR classes are very different (Figure 1). However, these loops have the same length. The first residue at position 154 and the last residue at position 167 are conserved. Charged residues at positions 157, 158, and 164 are also conserved or type-conserved. This suggests that the α8∩α9 loops from the two classes could have the same behavior. Although specific effects of the sequences cannot be ruled out, a possible explanation for the discrepancy between spectroscopic and crystallographic data is that the poorly defined electron density in $TetR^D$ results from static disorder arising from the existence of (at least) two macroconformations of the loop and not from dynamic disorder arising from a single highly flexible conformation. This is corroborated by the temperature dependence of the time-resolved fluorescence of Trp-162, Trp-163, and Trp-165, which indicated the existence of at least two conformations of the loop (*19*). The existence of slow interconverting loop conformations is commonly observed by NMR with exchange rates in the micro- to millisecond range (*1*).

In the absence of inducer, the Trp mobility on the picosecond time scale significantly increased at positions 164 and 165, albeit these positions did not have special spectral properties as compared to the other red-shifted positions (159, 160, 161, and 162) (Table 3). This suggests that this might arise from an increased flexibility of the backbone at these positions. In addition, the backbone mobility on the nanosecond time scale is higher at position 164. Although we cannot exclude a specific effect of the mutation introduced (Asp to Trp) on the mobility of the loop, it is noteworthy that positions 164 and 165 correspond to the limit of poorly defined electron density in the induced state (*8*−*9*) and in the inducer-free state (*10*), respectively. This suggests that the 164−165 positions might correspond to a hinge for conformational changes between different conformations of the loop. Increased mobility on the picosecond time scale at hinge positions have been observed for the triosephosphate isomerase, although the actual time scale for the hinge motion is slower by several orders of magnitude (*46*). In the complex with AnTc, the mobility on the picosecond time scale (S_{uf}^2) does not depend of the position, which might be related to the existence of a single loop conformation (see below).

(3) AnTc Effect on the Loop Dynamics. The effect of AnTc on the loop dynamics could be investigated only at positions for which the energy transfer efficiency was <0.80 (159, 162, 164, 165, and 167). At these positions, the fluorescence anisotropy decay was markedly altered upon AnTc binding to TetR and indicated an increased mobility (Table 4). The generalized order parameter for subnanosecond/nanosecond motions markedly decreased at these positions (Figure 7). In the presence of AnTc, four Trp (positions 159, 162, 164, and 165) have $S_g^2 \leq 0.5$, indicating high local flexibility of the loop backbone. The increased flexibility of the loop upon inducer binding is in contrast with the general behavior that ligand binding induces a damping of motion (*47*−*53*). However, more complex situations in which the mobility of some residues can increase or decrease upon ligand binding have also been reported. Molecular simulations have suggested that the binding of hexasaccharide to lysozyme may induce increased and decreased motions in different parts of the protein (*54*). Recently, NMR has provided an experimental evidence of increased and decreased backbone motions of lysozyme upon (NAG)3 binding (*55*). The binding of the competitive inhibitor *cis*,*cis*-muconate to 4-oxalocrotonate tautomerase increases the backbone S^2 of some residues and decreased the backbone S^2 of other residues (*56*). To explain this behavior, it has been proposed that the increased motions in some parts of the protein might partially compensate the entropy cost of "freezing" residues at the active site, yielding smaller overall entropy changes (*56*).

B-factors obtained for the inducer-free and -bound states indicate a greater flexibility of inducer-free TetR, especially for the α4∩α5 and α6∩α7 loops and α-helix 9 (*10*). The *B*-factors of α-helix 9 backbone residues are very large for a secondary structure element (up to 100 $Å^2$), suggesting structural heterogeneity, consistent with the different positioning of this helix in different protein states (*11*). In the induced state, the flexible regions are "frozen" by specific interaction with the inducer (*10*). In addition, the N-terminal part of the α8∩α9 loop is also "frozen" by a transition from a loop to an α-helix conformation (*10*). This indicates that the allosteric transition might have a very high entropic penalty. The increased mobility of the C-terminal part of the α8∩α9 loop might contribute to smaller entropy changes, according to the compensation mechanism proposed by Stivers et al. (*56*). The lack of inducibility of mutants whose α8∩α9 loop is immobilized via the formation of disulfide bonds between the loop and the protein core (DC106PC159′ and EC107NC165′ $TetR^D$) (*14*) might be related (at least in part) to entropic factors.

Very recently, it has been observed that the electron density of the α8∩α9 loop in $TetR^D$ complexed with AnTc and Mg^{2+} is sufficiently defined to allow structural determination, presently under refinement (W. Hinrichs, personal

communication). This indicates that, in the AnTc-bound state, the α8∩α9 loop has a single conformation. However, *in solution*, this conformation would be characterized by an increased backbone flexibility on the subnanosecond−nanosecond time scale, as compared to the inducer-free conformations.

In the absence of inducer, the α8∩α9 loop ranges from residues 151 to 167. In the presence of inducer, its length is shorter (residues 154−166), because of the extension of α-helix 8 (*10*). The C-termini of the loop in the inducer-bound and inducer-free states also have different positions, due to a 2 Å motion of α-helix 9 as a whole (*10*). The very different positions of the flanking residues indicate that the structure of the loop in the inducer-free and -bound states should be markedly different. The present study indicates that, in addition to structural reorganization, the backbone dynamics of the α8∩α9 loop is also markedly altered upon inducer binding.

CONCLUDING REMARKS

The Trp mutations carried out for this study do not impair Tet repressor inducibility and thus do not prevent the α8∩α9 loop motion necessary for induction. However, the possibility that they alter the loop mobility cannot be rigorously ruled out, in particular when they replace a proline (positions 161 and 167). Despite this limitation, which is inherent to any mutational study, several conclusions can be drawn from the similarities observed in the anisotropy decays at different positions: (1) the fluorescence anisotropy decay of a Trp residue in a protein is informative of the local backbone motion, (2) the α8∩α9 loop backbone has a limited flexibility in the absence of inducer on the picosecond/nanosecond time scale, and (3) anhydrotetracycline binding induces an increased flexibility of this loop. This latter point suggests that entropic factors might play an important role in the mechanism of allosteric transition.

ACKNOWLEDGMENT

We thank Professor W. Saenger and Dr. W. Hinrichs (Berlin, Germany) for critical reading of the manuscript and stimulating discussions.

REFERENCES

1. Jardetzky, O. (1996) *Prog. Biophys. Mol. Biol. 65*, 171−219.
2. Lipari, G., and Szabo, A. (1982) *J. Am. Chem. Soc. 104*, 4548−4559.
3. Kay, L. W., Torchia, D. A., and Bax, A. (1989) *Biochemistry 28*, 8972−8979.
4. Clore, G. M., Driscoll, P. C., Wingfield, P. T., and Gronenborn, A. M. (1990) *Biochemistry 29*, 7387−7401.
5. LeMaster, D. M., and Kushlan, D. M. (1996) *J. Am. Chem. Soc. 118*, 9255−9264.
6. Yang, D., Mittermaier, A., Mok, Y.-K., and Kay, L. E. (1998) *J. Mol. Biol. 276*, 939−954.
7. Hillen, W., and Berens, C. (1994) *Annu. Rev. Microbiol. 48*, 345−369.
8. Hinrichs, W., Kisker, C., Düvel, M., Müller, A., Tovar, K., Hillen, W., and Saenger, W. (1994) *Science 264*, 418−420.
9. Kisker, C., Hinrichs, W., Tovar, K., Hillen, W., and Saenger, W. (1995) *J. Mol. Biol. 247*, 260−280.
10. Orth, P., Cordes, F., Schnappinger, D., Hillen, W., Saenger, W., and Hinrichs, W. (1998) *J. Mol. Biol. 279*, 439−447.
11. Orth, P., Saenger, W., and Hinrichs, W. (1999) *Biochemistry 38*, 191−198.
12. Berens, C., Pfleiderer, K., Helbl, V., and Hillen, W. (1995) *Mol. Microbiol. 18*, 437−448.
13. Berens, C., Schnappinger, D., and Hillen, W. (1997) *J. Biol. Chem. 272*, 6936−6942.
14. Tiebel, B., Aung-Hilbrich, L. M., Schnappinger, D., and Hillen, W. (1998) *EMBO J. 17*, 5112−5119.
15. Müller, G., Hecht, B., Helbl, V., Hinrichs, W., Saenger, W., and Hillen, W. (1995) *Nat. Struct. Biol. 2*, 693−703.
16. Kintrup, M. (1997) in Konformationsanalyse des Tn*10*-kodierten Tet repressors durch singuläre tryptophanmutanten, Ph.D. Thesis, Friedrich-Alexander Universität, Erlangen, Germany.
17. Ettner, N., Müller, G., Berens, C., Barkes, H., Schappinger, D., Schreppel, T., Pfleiderer, K., and Hillen, W. (1996) *J. Chromatogr. 1742*, 95−105.
18. Brochon, J.-C. (1994) *Methods Enzymol. 240*, 263−311.
19. Alberti, P., Bombarda, E., Kintrup, M., Hillen, W., Lami, H., Piémont, E., Doglia, S. M., and Chabbert, M. (1997) *Arch. Biochem. Biophys. 346*, 230−240.
20. Cross, A. J., and Fleming, G. R. (1984) *Biophys. J. 46*, 45−56.
21. Peviani, C., Hillen, W., Ettner, N., Lami, H., Doglia, S. M., Piémont, E., Ellouze, C., and Chabbert, M. (1995) *Biochemistry 34*, 13007−13015.
22. Bevington, P. R. (1969) *Data Reduction and Error Analysis for the Physical Sciences*, McGraw-Hill, New York.
23. Silvi Antonini, P., Hillen, W., Ettner, N., Hinrichs, W., Fantucci, P., Doglia, S. M., Bousquet, J.-A., and Chabbert, M. (1997) *Biophys. J. 72*, 1800−1811.
24. Lipari, G., and Szabo, A. (1980) *Biophys. J. 30*, 489−506.
25. Lakowicz, J. R., Maliwal, B. P., Cherek, H., and Balter, A. (1983) *Biochemistry 22*, 1741−1752.
26. Burstein, E. Q., Vedenkina, N. S., and Ivkova, M. N. (1973) *Photochem. Photobiol. 18*, 263−279.
27. Van der Meer, B. W., Raymer, M. A., Wagoner, S. L., Hackney, R. L., Beechem, J. M.and Gratton, E. (1993) *Biophys. J. 64*, 1243−1263.
28. Levy, R. M., and Sheridan, R. P. (1983) *Biophys. J. 41*, 217−221.
29. Baici, A., Rizzo, V., Skrabal, P., and Luisi, P. L. (1979) *J. Am. Chem. Soc. 101*, 5170−5179.
30. Dezube, B., Dobson, C. M., and Teague, C. E. (1981) *J. Chem. Soc., Perkin Trans. 2*, 730−735.
31. Hu, J.-S., Grzesiek, S., and Bax, A. (1997) *J. Am. Chem. Soc. 119*, 1803−1804.
32. Ichiye, T., and Karplus, M. (1983) *Biochemistry 22*, 2884−2893.
33. Bremi, T., Brüschweiler, R., and Ernst, R. R. (1997) *J. Am. Chem. Soc. 119*, 4272−4284.
34. Lipari, G., and Szabo, A. (1982) *J. Am. Chem. Soc. 104*, 4559−4570.
35. Grasberger, B., Gronenborn, A. M., and Clore, G. M. (1993) *J. Mol. Biol. 230*, 364−372.
36. Yamasaki, K., Saito, M., Oobatake, M., and Kanaya, S. (1995) *Biochemistry 34*, 6587−6601.
37. Frauenfelder, H., Parak, F., and Young, R. D. (1988) *Annu. Rev. Biophys. Chem. 17*, 451−479.
38. Frauenfelder, H., Sligar, S. G., and Wolynes, P. G. (1991) *Science 245*, 1598−1603.
39. Elber, R., and Karplus, M. (1987) *Science 235*, 318−321.
40. Noguti, T., and Go, N. (1989) *Proteins: Struct., Funct., Genet. 5*, 97−103.
41. Noguti, T., and Go, N. (1989) *Proteins: Struct., Funct., Genet. 5*, 104−112.
42. Noguti, T., and Go, N. (1989) *Proteins: Struct., Funct., Genet. 5*, 113−124.
43. Troyer, J. M., and Cohen, F. E. (1995) *Proteins: Struct., Funct., Genet. 23*, 97−110.
44. Kitao, A., Hayward, S., and Go, N. (1998) *Proteins: Struct., Funct., Genet. 33*, 496−517.
45. Wittebort, R. J., and Szabo, A. (1978) *J. Chem. Phys. 69*, 1722−1736.
46. Joseph, D., Petsko, G. A., and Karplus, M. (1990) *Science 249*, 1425−1428.

47. Nicholson, L. K., Kay, L. E., Baldisseri, D. M., Arango, J., Young, P. E., Bax, A., and Torchia, D. A. (1992) *Biochemistry 31*, 5253−5263.
48. Akke, M., Skelton, N. J., Kördel, J., Palmer, A. G., III, and Chazin, W. J. (1993) *Biochemistry 32*, 9832−9844.
49. Cheng, J.-W., Lepre, C. A., Chambers, S. P., Fulghum, J. R., Thomson, J. A., and Moore, J. M. (1993) *Biochemistry 32*, 9000−9010.
50. Cheng, J.-W., Lepre, C. A., and Moore, J. M. (1994) *Biochemistry 33*, 4093−4100.
51. Fushman, D., Ohlenschläger, O., and Rüterjans, H. (1994) *J. Biomol. Struct. Dyn. 11*, 1377−1402.
52. Olejniczak, E. T., Zhou, M.-M., and Fesik, S. W. (1997) *Biochemistry 36*, 4118−4124.
53. Gryk, M. R., Abseher, R., Simon, B., Nilges, M., and Oschkinat, H. (1998) *J. Mol. Biol. 280*, 879−896.
54. Post, C. B., Dobson, C. M., and Karplus, M. (1989) *Proteins: Struct., Funct., Genet. 5*, 337−354.
55. Mine, S., Tate, S., Ueda, T., Kainosho, M., and Imoto, T. (1999) *J. Mol. Biol. 286*, 1547−1565.
56. Stivers, J. T., Abeygunawardana, C., Mildvan, A. S., and Whitman, C. P. (1996) *Biochemistry 35*, 16036−16047.

BI9912591